# Thermal Behavior of Materials in Laser-assisted Extreme Manufacturing: Raman-based Novel Characterization

Ridong Wang [a, 1], Shen Xu [b, 1], Yanan Yue [c, 1], Xinwei Wang [d, *]

[a] State Key Laboratory of Precision Measuring Technology and Instruments, Tianjin University, Tianjin 300072, People's Republic of China.

[b] School of Mechanical and Automotive Engineering, Shanghai University of Engineering Science, Shanghai 201620, People's Republic of China.

[c] School of Power and Mechanical Engineering, Wuhan University, Wuhan 430072, People's Republic of China.

[d] Department of Mechanical Engineering, Iowa State University, Ames, Iowa 50011, United States.

[*] Corresponding Author: xwang3@iastate.edu (X. Wang)

[1] These authors contributed equally to this work.

## Abstract

Laser-assisted manufacturing (LAM) is a technique that performs machining of materials using a laser heating process. The temperature rise in the process sometimes can be over 2000 °C. As a result, it is very crucial to explore the thermal behavior of materials under such high temperature to understand the physics behind LAM and provide feedback for manufacturing optimization. Raman spectroscopy, which is widely used for structure characterization, can provide a novel way to measuring temperature during LAM. In this review, we discuss the mechanism of Raman-based temperature probing in detail, its calibration, and uncertainty/error sources and control. We critically review the Raman-based temperature measurement considering the spatial resolution under near-field optical heating and surface structure-induced asymmetries. As another critical aspect of Raman-based temperature measurement - temporal resolution is also reviewed to cover various ways to realize ultrafast thermal probing. Detailed outlooks are provided about Raman-based temperature probing in LAM and issues that need special attention.

## 1. Introduction

Laser-assisted manufacturing (LAM) is a method that applies the instantaneous heating capability of laser with a focused beam to materials that are difficult to process by mechanical machining alone.[1-2] This method has been applied in various manufacturing processes, including drilling, cutting, turning, peening, nanoimprinting, additive manufacturing, scanning probing microscope, etc.[1, 3-10]

In the laser-assisted drilling (LAD) process, the laser beam is focused onto the workpiece surface to melt or evaporate the material, and an assisted gas is usually used to blow away the molten material or vapor. This technique is widely used in many areas such as heavy machinery, aerospace sectors, marine, chemical and automotive industries, etc.[5, 11] Similar to LAD, in the laser-assisted cutting process, the laser beam is also focused onto the material, and material around the focal point will melt and be blown away by the assisting cutting gas. This method has found applications in punching, cut-off and marking of metals, ceramics and plastics.[12]

Laser-assisted turning, which combines turning and laser heating, can be used as a good alternative to the grinding process of hard-to-manufacture materials. In this process, the laser is used to heat up the material in the cutting zone to reduce the material strength. Thus, the cutting force can be reduced significantly to result in significant machinability improvement. This process can also increase the productivity and accuracy, reduce installation spaces and energy consumption.[1, 13]

As an efficient thermo-mechanical approach to engineer and modify the surface and subsurface related properties of materials, laser peening has been widely used in aerospace, automotive,

shipbuilding, biomedical, microelectronics, and microelectromechanical systems.[7, 14] In the process, a pulsed laser is used to irradiate the surface to generate a shock wave. The recoil pressure/stress wave in the substrate will compress the substrate and achieve surface hardening.[15-17]

Laser nanoimprinting is a technique that utilizes a laser pulse to irradiate the sample surface. The sample surface is in contact with and pre-loaded by a mold (fused quartz) with pre-fabricated nanoscale features on its contact side. Upon irradiating the laser pulse on the sample surface, the near-surface materials melt and a laser-induced molten layer is formed, which allows the mold to impinge into the sample directly. The nano-patterns are transformed from the mold to the sample upon cooling and solidification of the molten layer.[18-19] This technique has been used widely for making photonic bandgap crystals.[20]

In recent years, laser additive manufacturing has attracted significant attention. It is a technology that uses the method of material accumulation to produce solid parts. The machining process is based on the CAD digital model to stratify the data of the material model, and then layer by layer to generate three-dimensional entities by laser processing. Two most typical techniques of this technology are selective laser melting technology and laser cladding deposition technology. In both techniques, the metal powder is melted by the laser to form the desired entity.[21] Laser additive manufacturing has been widely used in aerospace, medical, automotive, electronics, military and other fields.[21-25]

In laser-assisted scanning probing microscope (SPM, e.g. scanning tunneling microscope and

atomic force microscope) surface nanostructuring, a laser is irradiating the tip surface to form near-field focusing to an extremely small region (a few nm). The tip undergoes a thermal expansion upon pulsed laser irradiation, resulting in mechanical contact with the sample surface to form nano-indentation.[26-28] The tip could also act as a receiving antenna to collect laser energy and as a transmitting antenna to the tip to enhance the optical field by a few orders of magnitude. And the enhanced optical field can heat the sample surface to induce phase change or chemical reaction and modify the surface at the nanoscale.[26, 29-30]

All the above outlined processes involve intensive heating, which indicates that the heating level/material's thermal response is critical for understanding the physics behind the laser-assisted manufacturing, and for providing feedback for manufacturing optimization. The infrared thermometry technique is widely used for temperature measurement.[31-33] It measures the infrared thermal radiation from the heating region (sometimes if the temperature is very high, the measured radiation wavelength could be visible). But this technique is hard to measure the transient response of the sample, especially under ultrafast laser pulse heating or for regions that is too small to probe (like nanoscale/near-field manufacturing). A thermocouple-based technique can also be used to measure the temperature.[31, 34-36] The thermocouple is comprised of two dissimilar conductors to measure unknown temperature with reference to the known temperature. This contact technique has more limitations in terms of transient response, measurement capacity/range, and spatial resolution.

Raman spectroscopy, which is widely used for structure characterization, can also be used for temperature probing.[37-41] That is, this technique provides a novel way to measuring temperature

during laser-assisted extreme manufacturing, and can provide unique and unprecedented knowledge about the physics involved in laser extreme manufacturing. In the following sections, a comprehensive critical review about various Raman-based techniques that can be used for temperature probing is presented, with the aim of constructing a good picture of this field to our best knowledge.

## 2. Raman-based Temperature Probing

### 2.1 Mechanism of Raman scattering

In 1928, C.V. Raman first discovered the inelastic scatterings of photons from matter when photons of the incident light interacted with matter.[42-43] These inelastic scatterings, termed Raman scatterings, originate from the change in polarizability of vibrational modes of chemical bonds in molecules, which is the instant deformity of the electric dipole of molecules due to the incidence of an electromagnetic field.[44-45] The electric dipole moment $\mu$ is proportional to the incident electric field with a polarizability *a*, and has an expression as followings.[45]

$$\mu = a_0 E_0 \cos\omega_0 t + \frac{1}{2}\left(\frac{\partial\alpha}{\partial q}\right)\Big|_{q=0} \cdot q_0 E_0 \cos\left(\omega_0 - \omega_R\right)t + \frac{1}{2}\left(\frac{\partial\alpha}{\partial q}\right)\Big|_{q=0} \cdot q_0 E_0 \cos\left(\omega_0 + \omega_R\right)t, \qquad (1)$$

where $E_0$ is the incident electric field, $\omega_0$ and $\omega_R$ are the frequencies of the incident photons and vibrational mode, $a_0$ is the original polarizability, and $q$ is the nuclear motion. On the right side in Equation (1), the first term stands for Rayleigh scatterings, the second term is for Stokes scatterings, and the third term is anti-Stokes scatterings, as shown in Fig. 1.

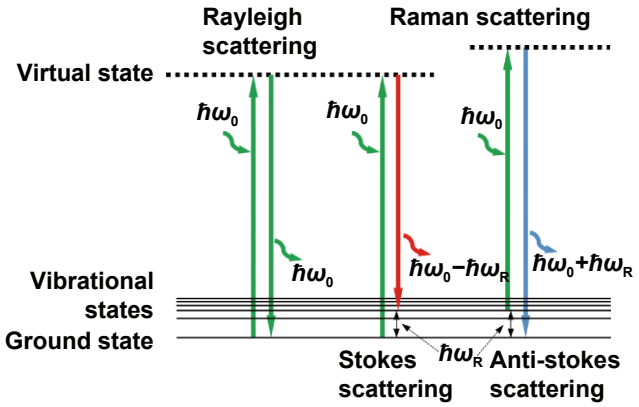


Figure 1. The mechanism of Stokes and anti-Stokes scatterings generation.

The Stokes scatterings arise when the chemical bonds absorb the incident photon energy ($h\omega_0$), the electrons are excited to a virtual state, then de-excited to an excited state, and emit new photons with a lower energy ($h\omega_0 - h\omega_R$).[46] Different from the Stokes scattering, anti-Stokes scatterings occur when electrons at an excited state is excited to the virtual state, then return to the ground state, and emit photons. The scattered photons gain energy from the molecules and have a higher energy than the incident ones as ($h\omega_0 + h\omega_R$).[47] The amount of energy gained or lost by the vibrational modes ($h\omega_R$) only depends on its nucleus mass and the strength of the chemical bonds involved in the Raman scattering. Therefore, the frequency shift ($\omega_R$) of Raman scatterings, either Stokes or anti-Stokes, would be uniquely related to a specific chemical bond, and the corresponding Raman spectrum is featured to be "fingerprint". Since the Raman scatterings respond to the change in vibrational modes of chemical bonds, they would vary as vibrational modes are changing along with the environment, such as temperature and stress. Therefore, temperature can be measured base on the changes in Raman spectra, which is termed Raman thermometry.[48]

### 2.2 Raman-based temperature probing

Temperature variation of the tested sample will affect the properties of its Raman peaks, when other measuring conditions are well controlled. To be specific, take a Stokes Raman peak as an example, its Raman wave number red shifts, intensity decreases, and linewidth broadens as the temperature goes higher.[49-51] In a certain temperature range of approximate 50 degrees variation,[52-53] the changing rates/temperature coefficients of these three properties could be safely assumed constant. Thus, the temperature can be determined based on a linear relation.

#### 2.2.1 Temperature response of Raman peaks

Raman shift is the mostly adopted property for temperature measurement in Raman thermometry. It originates from dipoles in chemical bonds of materials and its value directly indicates the specific structure in the material. For the fact that the temperature rise will vary the energy and thus the frequency of the vibrational mode, Raman shift responds to temperature sensitively. Raman shift moves to a lower value, or red shifts, as temperature goes higher, while it blue shifts when temperature decreases. Variation of Raman shift against temperature for Stokes peaks has the following expression.[54]

$$\omega(T)=\omega_0+A\left(1+\frac{2}{e^{\frac{h\omega_0}{4\pi kT}}-1}\right)+B\left(1+\frac{3}{e^{\frac{h\omega_0}{4\pi kT}}-1}+\frac{3}{(e^{\frac{h\omega_0}{4\pi kT}}-1)^2}\right), \tag{2}$$

where $h$ and $k$ are Planck constant and Boltzmann constant, $T$ is the absolute temperature, $A$ and $B$ are constants specific to materials. However, besides temperature, stress will also affect the exact value of Raman shift because the stress-induced strain will also alter the bond force and hence the energy and frequency of the vibrational mode as the temperature effect does. In laser-assisted extreme manufacturing, a large temperature rise occurs in the irradiated area and causes a large

temperature gradient around the laser spot. An accompanied high thermal stress would correspondingly induce additional Raman shift on top of the temperature-induced one. In this case, the stress-induced Raman shift should be carefully evaluated when determining temperature using Raman shift.

The Raman linewidth is an alternative parameter to determine the temperature in the high stress case, for it depends on the lifetime of optical phonon in materials and is much less affected by stress. It is reported that temperature rise is accompanied by a decrease in phonon lifetime and thus a broadening in Raman linewidth. The mathematical expression of the Raman linewidth $\Gamma$ against temperature is:[54]

$$\Gamma(T) = C\left(1 + \frac{2}{e^{\frac{h\omega_0}{4\pi kT}} - 1}\right) + D\left(1 + \frac{3}{e^{\frac{h\omega_0}{4\pi kT}} - 1} + \frac{3}{(e^{\frac{h\omega_0}{4\pi kT}} - 1)^2}\right). \quad (3)$$

$C$ and $D$ are the constants depending on materials. Though the linewidth is exclusively dependent on temperature, it is less sensitive to temperature change compared with the Raman shift. It could be a good temperature indicator when Raman scatterings are sound enough to be well fitted using a Gaussian/Lorentzian shape.

The intensity of Raman scatterings, both Stokes and anti-Stokes, depends on the populations of their initial states. Stokes scatterings from a lower initial state have a larger population than that of anti-Stokes scatterings from an upper state according to the principle of thermodynamic equilibrium. Thus, Stocks scatterings are much stronger than anti-Stokes in the spectrum. Both will vary along with temperature. The ratio of Stokes to anti-Stokes could directly reveal the absolute temperature of the sample.[54]

$$\frac{I_s}{I_{as}} = \frac{\alpha_0 + \alpha_s}{\alpha_0 + \alpha_{as}} \left( \frac{\omega_0 - \omega_R}{\omega_0 + \omega_R} \right)^4 \exp\left( \frac{h\omega_R}{2\pi kT} \right), \quad (4)$$

where $\alpha_0$, $\alpha_s$, $\alpha_{as}$ are the absorbance regarding the incident photon frequency, Stokes frequency and anti-Stokes frequency, respectively. However, the Stokes and anti-Stokes peaks are hardly exhibited in one spectrum at the same time based on current spectroscopy techniques. Researchers used the Stokes scatterings more often than the ratio of the intensity to measure temperature.

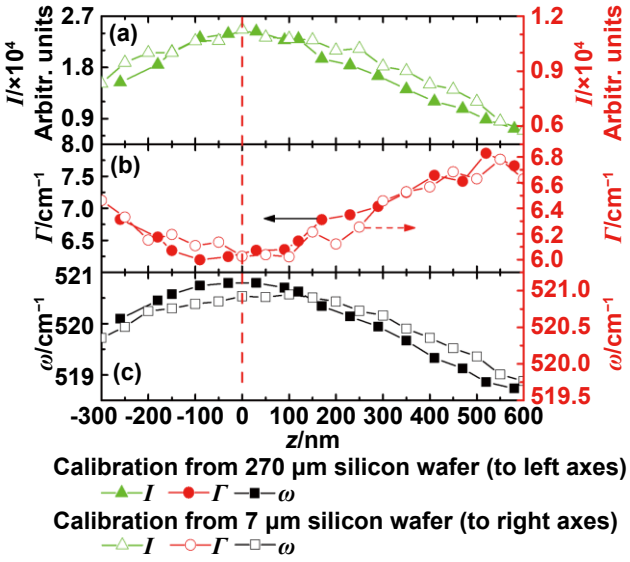


Figure 2. Out-of-focus effect induced variations in the intrinsic properties of the 521 $cm^{-1}$ peak of silicon. Red dash line crossing $z$=0 denotes the focal plane. (a) Raman intensity ($I$), (b) Raman linewidth ($\Gamma$), and (c) Raman shift ($\omega$) for the 521 $cm^{-1}$ peak.[55]

### 2.2.2 Optical focusing and out-of-focus effect on temperature measurement

For the reason that Raman scatterings are much weaker than Rayleigh scattering, around $10^{-8}$, a focusing system and a long-enough integration time are employed to increase the efficiency of Raman scattering acquisition.[55] However, these operations will bring up another important issue, out-of-focus effect due to stage drift, that should be carefully addressed before temperature measurement. Xu *et al.* has conducted a study of the out-of-focus effect on Raman spectra using commercial silicon wafers with thicknesses of 270 μm and 7 μm, respectively, under a 100×

microscope objective.[56] The silicon wafer was manually moved away from the focused level to obtain Raman spectra at different *z* positions. Figure 2 shows the variation of Raman properties of silicon's 521 $cm^{-1}$ peak against the *z* position.

Figure 2 shows that Raman intensity is decreasing, Raman shift is red-shifting, and linewidth is broadening as the sample surface leaves the focal plane until the out-of-focus effect could be directly observed as blur images through the imaging system by naked eyes. It has a similar trend as Raman peaks varies along with temperature elevation, and will cause undesired errors in temperature measurement. Taking the Raman shift as an example, the out-of-focus effect induced a shift of 0.1 $cm^{-1}$ when the surface moved away 90 nm from the focal level. This shift of 0.1 $cm^{-1}$ is equivalent to around 7 degrees' temperature rise in silicon based on the temperature coefficient of 0.015 $cm^{-1}/K$ in previous work.[54] Thus, in Raman thermometry, maintaining the sample's surface at a very well-focused level plays an extremely important role in measurement accuracy.

In previous work, thermal expansion was identified as one of the main reasons in practical experiments accounting for the unexpected shift of the sample surface away from the focal plane. It has two contributors, the sample and the sample stage.[57-58] When the heating laser is focused on the sample surface and heats the sample up, the sample will expand in both vertical and horizontal directions and the sample's surface moves away from the focal plane. The thermal expansion depends on the thickness and is $\Delta L = \alpha \cdot L \cdot \Delta T$ , where $\alpha$ is the thermal expansion coefficient.

The thermal expansion coefficient of most materials is in the order of $10^{-6}$ $K^{-1}$.[59] For suspended film-like materials, such as suspended graphene and other 2D materials, it is safe to neglect the thermal expansion as the samples are just several nanometers thick. However, in laser-assisted

extreme manufacturing, large temperature rises and thick materials may cause non-negligible thermal expansion and further cause the drift of the sample's surface out of the focal plane in the thickness direction. Furthermore, the sample stage which holds the sample in the manufacturing will also be affected by the elevated temperature in the sample and thermally expand. Though the temperature rise in the stage will not be as high as that in the sample, the centimeter-thickness of the stage will raise a large thermal expansion in the stage which causes the sample moving out of focal plane. Researchers have made great efforts to maintain the sample at the focal level, either monitoring samples simultaneously in an optical imaging system or developing self-focusing systems,[60-62] etc., to reduce the out-of-focus effect to the greatest extent.

### 2.3 Unique advantage of Raman thermometry: material-specific

Raman spectroscopy records the Raman scatterings, vibrational information about all the chemical bonds, in the excited/irradiated area by the incident laser. The "fingerprint" feature of Raman peaks enables all the peaks discretely exhibiting in one spectrum since the Raman peak is narrow enough. This is a great feature of Raman thermometry that it could distinguish all materials in the irradiated area and measure each material's temperature at the same time as long as their scatterings could be detected. Along with the prosperous of heterogeneous structure, Raman thermometry has been widely applied to temperature and thermophysical properties measurement of multiple materials involved. Take supported 2D materials as an example, it could probe the temperatures of both the 2D materials and the substrate.[63] While for laser assisted nanostructure manufacturing, though the structure is smaller than the incident laser spot, its Raman scattering still could be measured in Raman thermometry. This could detect the chemical process of precursors and measure their temperature in laser-assisted manufacturing, such as laser-assisted chemical vapor deposition and additive manufacturing,[64-65] to better monitor the manufacturing process and optimize the structure.

As the Raman excitation laser could penetrate into part of the tested sample in the thickness direction, Raman scatterings are generated not only from the surface but also in the volume across this thickness. Therefore, the measured temperature based on Raman thermometry is an intensity-weighted temperature over the volume, to be specific, over the depth and the irradiated area.[61, 66] The penetration depth $\tau$ depends on the wavelength of the incident laser $\lambda$ and the extinction coefficient $k$ of the material as $\tau = \lambda / 4\pi k$. The penetration depth of silicon is calculated to be 820 nm under the excitation of 532 nm laser at room temperature. Additionally, the Raman scatterings in the irradiated area are not evenly distributed for the reason that the optical intensity of the incident laser has a Gaussian profile in the irradiated area. Therefore, a Raman-intensity weighted average temperature, $\Delta\overline{T} = \iiint \Delta T I_{Raman} dV / \iiint I_{Raman} dV$, has been proposed to fully consider this volume effect.

### 2.4 Calibration and its uncertainty

#### A. Case-based calibration

In Raman based temperature measurement, calibration is needed to know the temperature coefficient of Raman properties, like Raman shift, Raman intensity, and Raman linewidth. In a relative narrow temperature range, the coefficients of the properties against temperature could be assumed linear based on previous research.[52, 54] To calibrate these temperature coefficients, a typical approach is to place the sample on a heating stage which is precisely temperature-controlled by a thermal probe.[49, 63, 66] The temperature of the stage is then raised step by step and a corresponding Raman spectrum is recorded at each temperature step. By using Gaussian/Lorentzian function fitting, the exact values of each type of the Raman intrinsic

properties are plotted against temperature to evaluate the slope of the linear curve, which is defined as the temperature coefficient for the Raman properties.

However, this calibration cannot be universal. If the material structure varies or the measuring condition changes, another calibration will be required. For example, graphene has been extensively studied using Raman spectroscopy in various fields, the temperature coefficient, instead of a fixed value, has been observed as diverse values mainly ranging from -0.015 to -0.076 $cm^{-1} \cdot K^{-1}$.[67-69] The structure of graphene samples, surrounding medium, and even the measurement condition will cause differences/errors in the calibrated temperature coefficients. The temperature coefficient of Raman shift of G peak was determined to be -0.016 $cm^{-1} \cdot K^{-1}$ for a single-layered graphene and -0.015 $cm^{-1} \cdot K^{-1}$ for a bilayered sample.[70] In the cases of both suspended and supported graphene, the temperature coefficients of the Raman properties are also different. The coefficient was reported to be -0.015 $cm^{-1} \cdot K^{-1}$ for a suspended sample,[71] -0.031 ± 0.005 $cm^{-1} \cdot K^{-1}$ for a supported one on $SiO_2$ substrate,[72] and -0.089 $cm^{-1} \cdot K^{-1}$ for one on copper.[73] Furthermore, it has been reported that the temperature coefficient for the G peak differs under different wavelengths of excitation lasers.[67-69, 74] Therefore, it is necessary to conduct calibration for each sample in a defined Raman system and the experiment temperature range should be well covered in calibration.

**B. Thermal expansion and stress effect in calibration**

In addition to the sample's conditions, the process of Raman scattering acquisition will inevitably introduce errors. As abovementioned, thermal expansions in both the sample and heating stage will shift the sample's surface away from the focal level and cause extra errors due to the out-of-focus effect. On the other hand, this could be manually minimized through re-focusing the sample.

Other errors arise because of temperature rise in the collecting objective and its surrounding air. Heat will automatically dissipate from the hot sample's surface to the cooler objective and surrounding air. This may account for the variation in the temperature coefficient for the same sample. In Wang's group, the temperature coefficient of c-Si has been calibrated multiple times, and the reported value is ranging from -0.019 to -0.0355 $cm^{-1} \cdot K^{-1}$ in different works.[60-61, 66] It is inevitable that the top layer (2D material) and the local interface spacing could introduce some extra shift of the Raman wavenumber due to be deflection of the back-scattered Raman beam, accounting for these reported widely scattered temperature coefficients of Raman wavenumber.

Moreover, the different scenarios in the measurement and calibration will also raise errors/deviations in temperature measurement, especially for layered materials. It was less considered before Tang *et al*. studied the thermal behaviors of supported graphene and found this phenomenon.[57-58] In the temperature measurement, the incident laser was focused on the sample's surface and heated the sample from the top. The focused heating spot raised a temperature gradient and generated thermal stress in the graphene layer. Moreover, the temperature rise in the graphene layer was higher than that in the substrate. This was due to two factors. One was the interface thermal resistance which impeded part of heat conduction through the interface. The other was that the substrate was a bulk, which could easily conduct heat away and minimize heat accumulation and further temperature rise. Two materials thermally expanded differently, and due to the mismatch at the interface, the substrate would build up another tensile stress in the graphene.

On the contrast, in the calibration both the graphene layer and substrate were heated evenly on the heating stage. The temperature also distributed uniformly in the graphene layer and no temperature gradient and thermal stress existed then. Moreover, the graphene layer and substrate had the same

temperature. Though there is still thermal expansion mismatch, the mismatch-induced stress that the substrate places on the graphene would definitely be different from that in the interface characterization. This difference between the measurement and calibration could cause finite, yet sometimes nonnegligible errors in the determined temperature and is hardly to exclude. Tang *et al.* utilized the different sensitivities of Raman shift and linewidth in responding to stress, and successfully deconjugated and quantified the temperature field and stress field, respectively.[57-58]

**C. Additional consideration in laser extreme manufacturing**

In the case of laser-assisted extreme manufacturing, a high temperature rise usually occurs in the irradiated area. Temperature determination based on the calibrated temperature coefficient could not be satisfied. This is because that the temperature coefficient is regarded as a constant in a narrow temperature range within 50 K but it becomes nonlinear for a wider temperature range.[52, 54] The assumption of constant temperature coefficient is not safe and may bring errors in temperature determination. Besides, if the heated region has a very high stress, raised either by the large temperature gradient or the thermal expansion mismatch at interfaces, the stress will affect the Raman shift greatly. While in calibration, the heating is uniform, and no stress is involved.[66] Therefore, to consider the stress effect, it will be great to combine the Raman shift and linewidth for temperature measurement. This could also help determine the local stress.

Another issue has been less considered in common Raman thermometry but should be addressed in laser-assisted extreme manufacturing is that usually the Raman intensity goes down against increased temperature. When temperature is very high, the Raman peaks could become too weak to detect, not to mention temperature measurement based on the properties of Raman peaks. One

way to overcome this problem is to employ resonance Raman spectroscopy to enhance the intensity of Raman scatterings, in which the incident photon energy of the Raman excitation laser is coincidence with the energy of a selected electronic transition. The vibrational modes under this resonance electronic excitation will show a $10^6$- to $10^8$-fold increment in polarizability and hence Raman intensity over spontaneous Raman.[55] It will help a great deal to achieve temperature measurement in the elevated temperature range in laser-assisted manufacturing.

## 3. Raman-based Thermal Probing in Near-field Laser Manufacturing

In near-field laser manufacturing, the distance between the laser-focusing feature and material of processing is very small, even less than 10 nm. In addition, the laser focal spot is in the same order of size. Thus, it is very difficult to characterize the temperature and stress of the laser-heated material. As the Raman signal is related to the temperature and structure of material, near-field Raman-based thermal probing, which is a non-contact technique with high resolution, can be used in such situation. In addition, the Raman-uncovered temperature and stress field can be used to study the effect of various physical parameters, including laser power, polarization, wavelength, the focal level, and pulse width. That is, the near-field Raman thermal probing technique holds a high potential for parameters optimization of near-field laser manufacturing.

### A. Temperature response of the substrate under nano-tip nearfield heating

The near-field technology has been demonstrated to be very effective in laser-assisted manufacturing at extremely small scales. Tip-induced near-field effect can focus the laser power to sub-10 nm regime with much enhanced laser energy intensity for heating and manufacturing. Previous section presents the principle of temperature measurement by using Raman scattering

signal, termed Raman thermometry. Considering this, we combined the tip enhanced near-field effect and the Raman thermometry to achieve the extreme temperature measurement during the nanoscale laser manufacturing. As a matter of fact, Raman signal of sub-10 nm regime at the focused area is greatly enhanced due to the enlarged scattering effect.[75] Thus, the Raman thermometry can be regarded as a promising tool for conducting thermophysical study in such extreme manufacturing scenario.

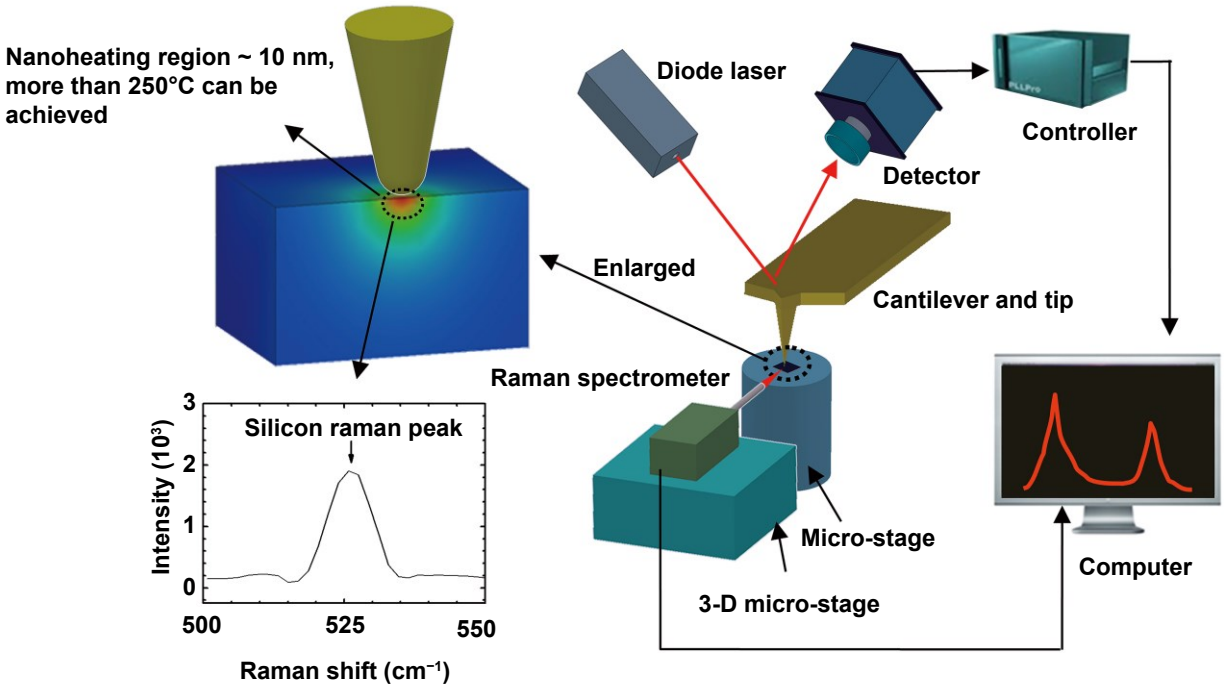


Figure 3. Experimental setup for tip-induced laser heating and temperature measurement based on Raman spectrum.[75]

Figure 3 shows the experimental setup for this tip-induced laser heating and temperature probing. The setup is built based on the AFM platform which can easily achieve precise control of tip-substrate distance.[75] It is well known that the tip-substrate distance is very important for near-field focusing of laser energy. In the operation, the contact mode of the AFM is set for the tip and substrate interaction since the laser enhancement can achieve the largest level, which also leads to the maximum of Raman signal enhancement. Strong Raman signal is very critical for successful

nanoscale thermal probing. Besides, the polarization angle is also very important to the near-field enhancement effect. Previously, we have validated that different polarization angle of the incident laser can lead to much difference in optical enhancement.[76] Figure 4 shows the simulation results for electric field distribution around the tip apex for the tip-substrate distance of 6 nm and tip radius of 30 nm. It is found that the enhancement regime is confined within around 10 nm scale and results in Fig. 4(d) indicate that the enhancement factor would be decreased rapidly as the polarization angle is larger than 30°.

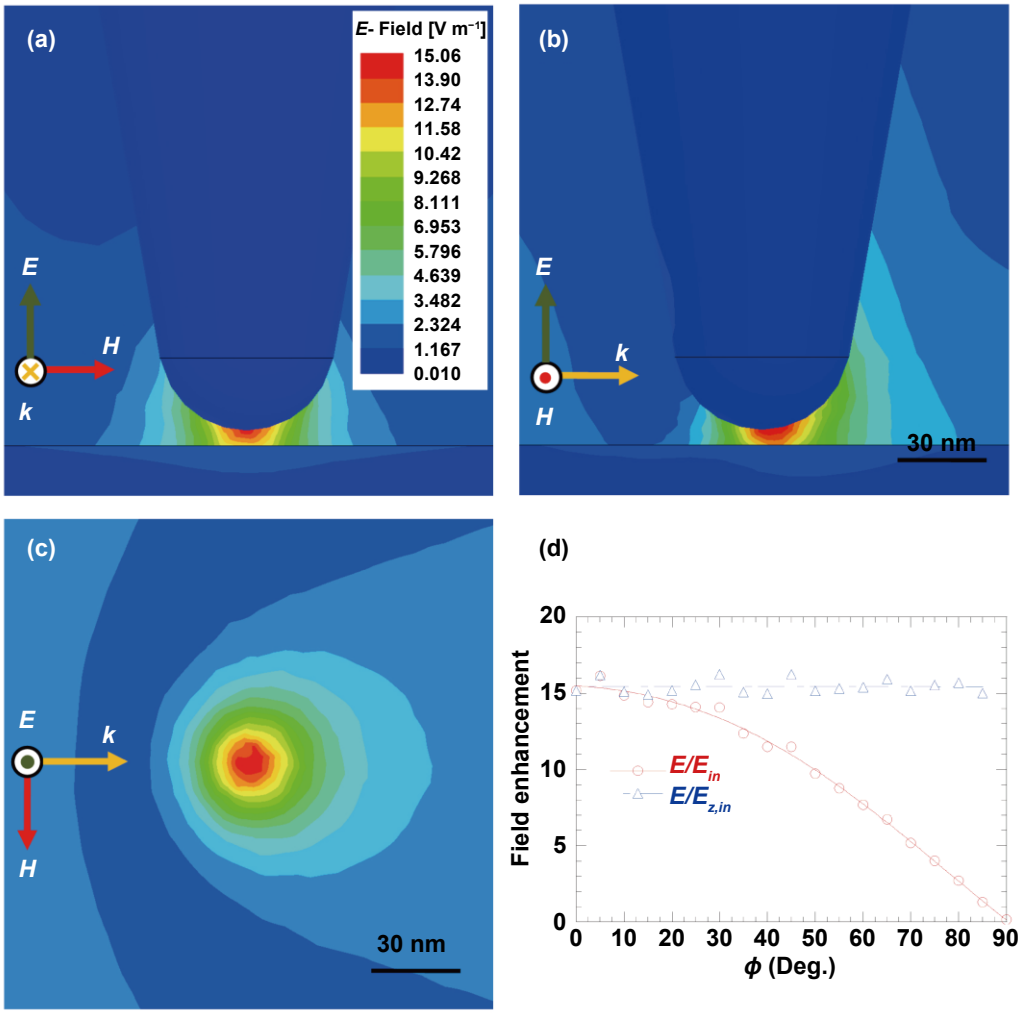


Figure 4. Electric field distribution around the tip apex for (a) the front view in the *y*–*z* plane and (b) the side view in the *x*–*z* plane, and (c) the top view of the cross-section under the tip apex; (d) field enhancement for different polarization angles.[76]

**B. Heating of nano-tip under laser irradiation**

The heating sources can vary from continuous laser to pulsed laser which features much more intense heating density. However, the heating effect of the tip should be carefully considered because of the high energy density of the laser could result in distinct temperature rise of the tip. Thermal stress and expansion effect of the tip due to large temperature rise could greatly modify the distance between the tip and substrate and thus, changes the scenario of near-field optical enhancement. Chen *et al*. studied that the temperature rise of the tip under pulsed laser heating (2.5 $mJ \cdot cm^{-2}$), as shown in Fig. 5.[76] As the thermal expansion is directly related to the temperature distribution along the tip, the temperature evolution of the tip apex should be evaluated with much caution.

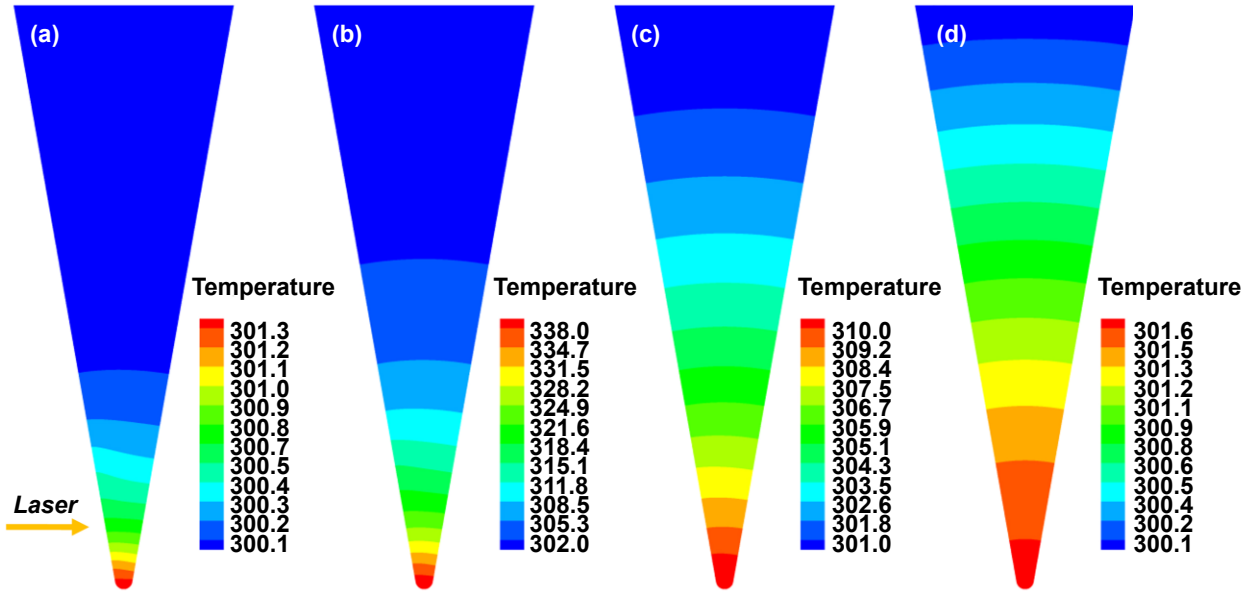


Figure 5. Temperature distribution of the tip at (a) $t$=10 ns, (b) $t$=20 ns, (c) $t$=30 ns, and (d) $t$=40 ns.[76]

Raman thermometry is not only effective for studying the tip-substrate interaction, but also an effective tool for probing the temperature rise of the tip itself. Most kinds of tips are made of silicon, which has a strong Raman peak at 520 $cm^{-1}$ in the spectrum. During the nanotip induced

extreme manufacturing, the temperature rise of nanotip would result in the deformation or even thermal failure. The temperature monitoring could provide an important guide to the engineering applications. In 2011, Wang's group reported the experimental observation of temperature rise of silicon nanotip under continuous wave (CW) laser irradiation.[77] As shown in Fig. 6, they reported that the temperature rise of the tip and cantilever were 754 and 626 K, respectively, under the laser heating density of $5.6\times10^{8}$ $W\cdot m^{-2}$. Such high temperature rise is attributed to the optical enhancement around the nanotip as well as the reduced thermal conductivity of the nanotip due to the inefficient phonon transport.

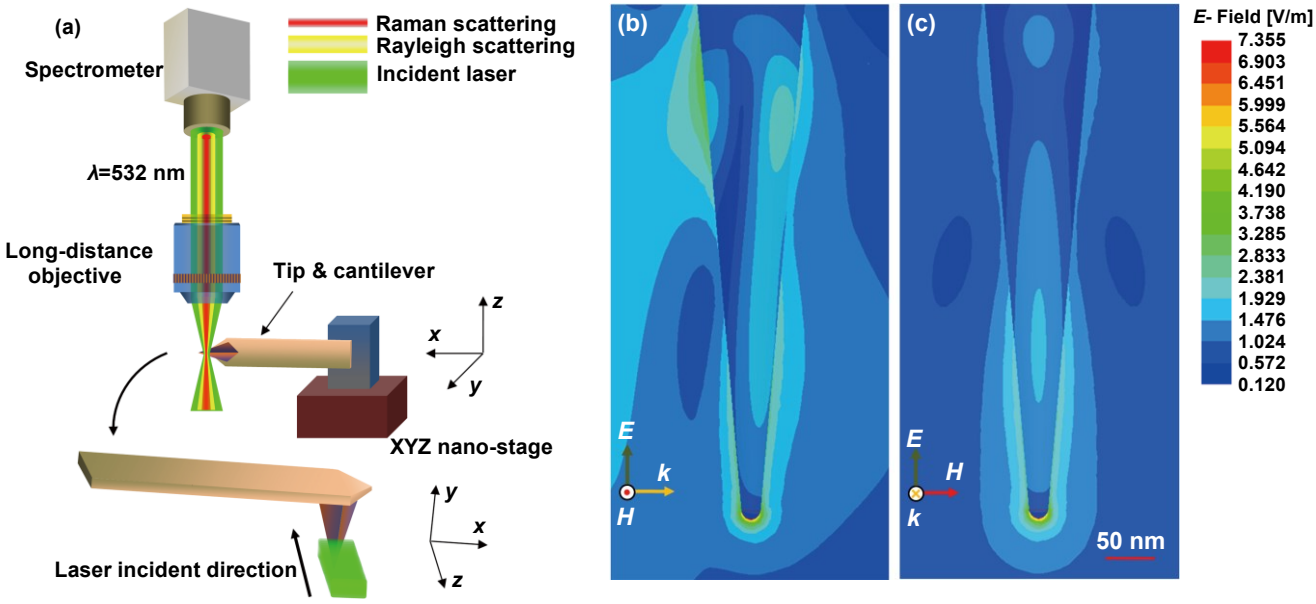


Figure 6. Thermal response of Si nano-tip to laser irradiation: (a) experimental setup for laser heating and Raman probing; (b) front- and (c) side- view of the simulation results of near-field enhancement around the tip.[77]

### C. Nearfield optical heating induced by micro/nanoparticles: conjugated physics probing

Besides the nanotip, nanoparticles are the other commonly used feature for inducing the near-field optical enhancement. There are many applications, for example in biomedical field, gold nanoparticles have been used as the nanoscale heating sources for killing cancer cells based on

their plasmonic effect under laser heating.[39, 78-80] Nanoparticles can also be used as imaging implement to break the diffraction limit combined with Raman scanning. Figure 7 shows the experimental setup for thermal imaging of nanoparticle induced near-field heating: the size of nanoparticle is comparable to or smaller than the wavelength of the laser (e.g. 532 nm).[81] The geometry of patterned nanoparticle is not observable under the microscope due to the diffraction limit. However, due to the near-field effect generated from the nanoparticle, the enhanced Raman signal from the substrate would show much difference as the Raman scanning proceeds. Actually, the Raman intensity profile shows excellent accordance with the size of nanoparticles. As shown in Fig. 7, the patterned nanoparticles (silica) are placed on silicon, and the movement of sample is controlled by a piezo-actuated nano-stage for precise controlling. Due to near-field effect, the region beneath the particle would be heated and such heating effect would appear as Raman shift of silicon peaks, as shown in Fig. 7 (c). It is known that the Raman spectrum shifts to left due to laser heating, stress, and out-of-focus effect. Distinguishing these effects is very challenging due to this small heating region (less than 100 nm), but is critical to the evaluation of thermophysical process of nanoparticle induced near-field heating.

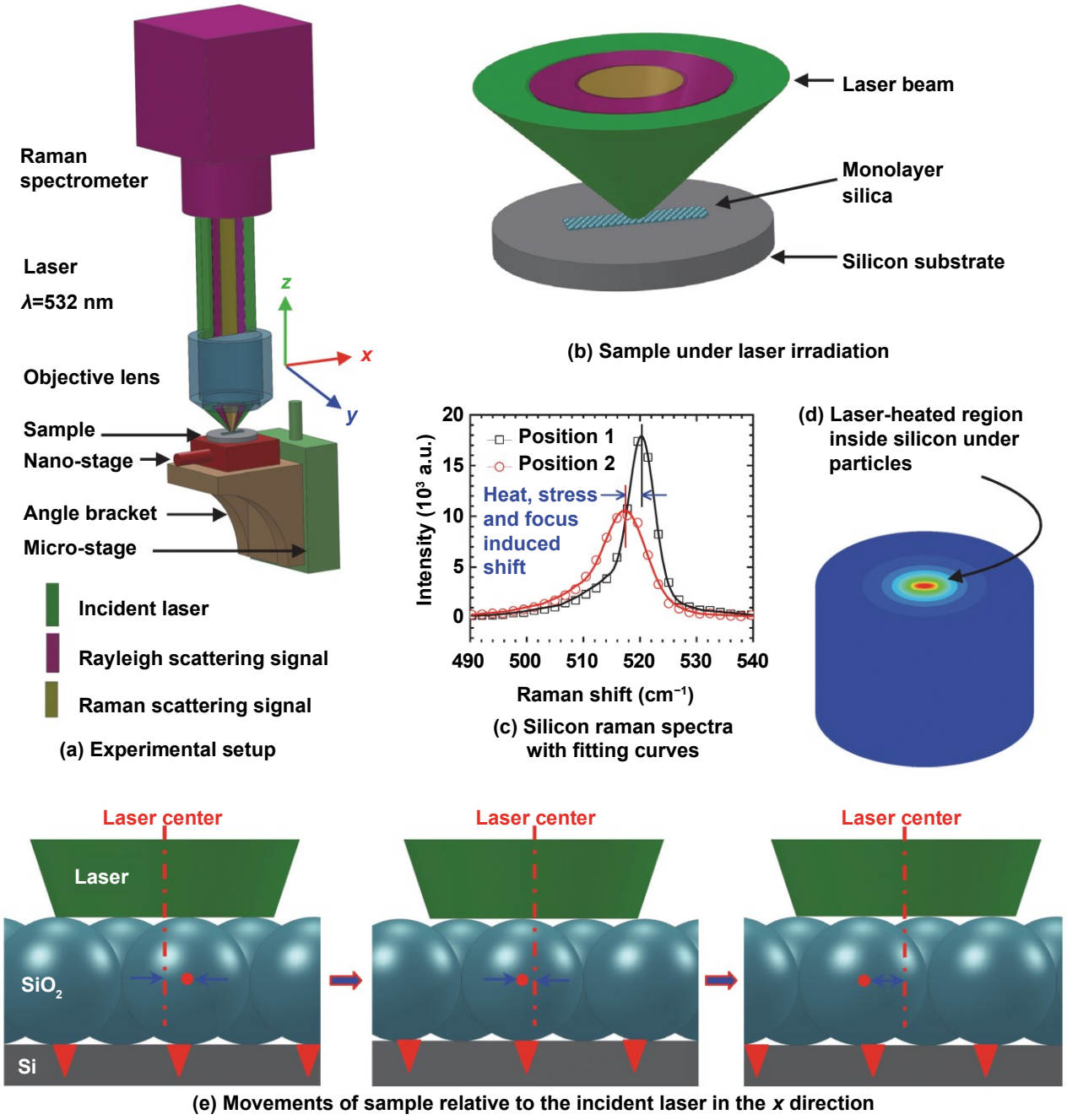


Figure 7. Nanoscale mapping of particle-induced thermal, stress, and optical fields.[81]

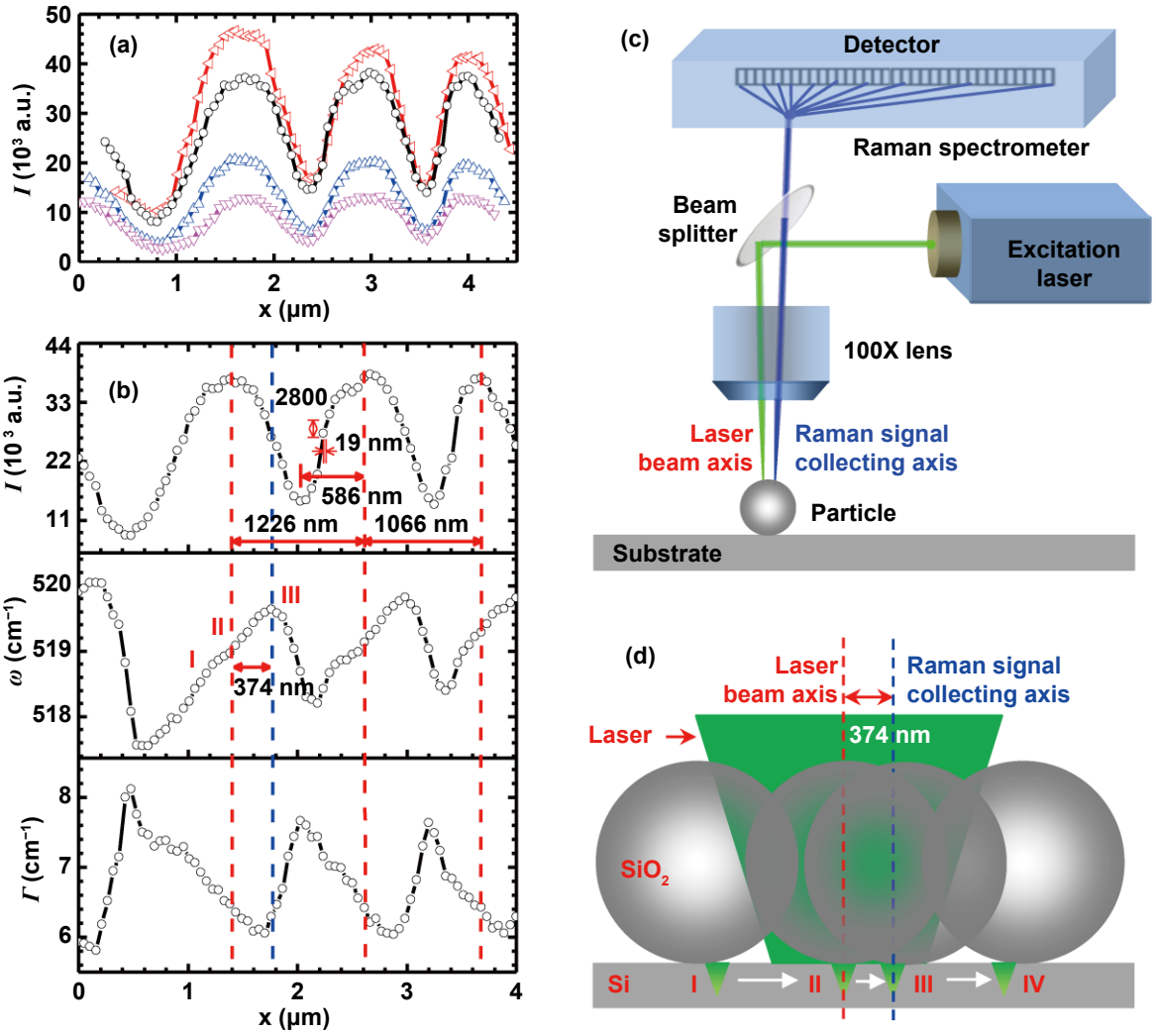


Figure 8. Nanoscale mapping for near-field heating under 1210 nm particles.[81]

As a matter of fact, Raman intensity, linewidth and Raman shift contain comprehensive information about the light-matter interaction, such as stress, temperature rise and so on. In applications of Raman thermometry, Raman shift properties are widely used for determining the temperature of target material.[49] However, the shift can also be caused by the strain effect due to the stress which brings some errors into the analysis. The linewidth is not significantly dependent on temperature, and temperature is a major factor affecting the linewidth. Thus, the Raman shift and linewidth can be used to build the spatial distribution of temperature and stress at the

nanoscale.[57]

Raman intensity is affected by three factors and can be expressed as $I \sim f_1 f_2 f_3(\Delta T)$, where $f_1$ denotes the system alignment factor, $f_2$ represents the intensity change due to laser energy, and $f_3(\Delta T)$ is the intensity variation caused by the temperature. In order to determine the thermal stress ($\sigma$) inside substrate, combined analysis of Raman wavenumber ($\omega$) and linewidth ($\Gamma$) is needed. As shown in Fig. 8, $\omega$ decreases and $\Gamma$ broadens as temperature increases. It is noted that $\Gamma$ has lower temperature sensitivity than $\omega$ and $\Gamma$ is stress insensitive to the first order, while stress causes a shift in $\omega$. Tang *et al.* reported that their mapping results based on Raman intensity variation, wavenumber shift, and linewidth broadening all give consistent conjugated thermal, stress, and near-field focusing effects at a 20 nm resolution.[81] This high spatial resolution is not determined by the wavelength of light sources but determined by the resolution of the piezo-actuation of the nano-stage. In their work, the Raman intensity difference can be distinguished over a distance of 20 nm in the sample moving direction, meaning the spatial resolution can reach this high level.

**D. Asymmetries during Raman scanning of surface nanostructures**

It needs to be noticed that the Raman scanning method is only based on some ideal cases such as very flat/even surface, which means if there is structure variation in space, this structure variation will cause Raman intensity and wavenumber change. Such change cannot be simply taken as temperature and stress effect. Therefore, the structure variation/distribution in space must be taken into serious consideration in scanning Raman for stress and temperature measurement. Besides, the asymmetries of Raman scattering along one scanning direction, and between two scanning directions should be considered. Such asymmetries are mainly caused by the alignment of the

detector units in the spectrometer and the pixel numbers along each direction. For 2D materials, such as $MoSe_2$ nanosheet, in addition to the asymmetry of Raman shift when scanned along the two directions, a third asymmetry, which was caused by the step variation of the sample edge, was also discovered by Wang *et al*.[82] To address these issues, as shown in Fig. 9, Wang *et al*. reported a data construction method to eliminate these asymmetries.[82] In this method, the Raman signals along -*x* and +*x* directions, and along -*y* and +*y* directions at the corresponding positions are averaged to eliminate the asymmetries.

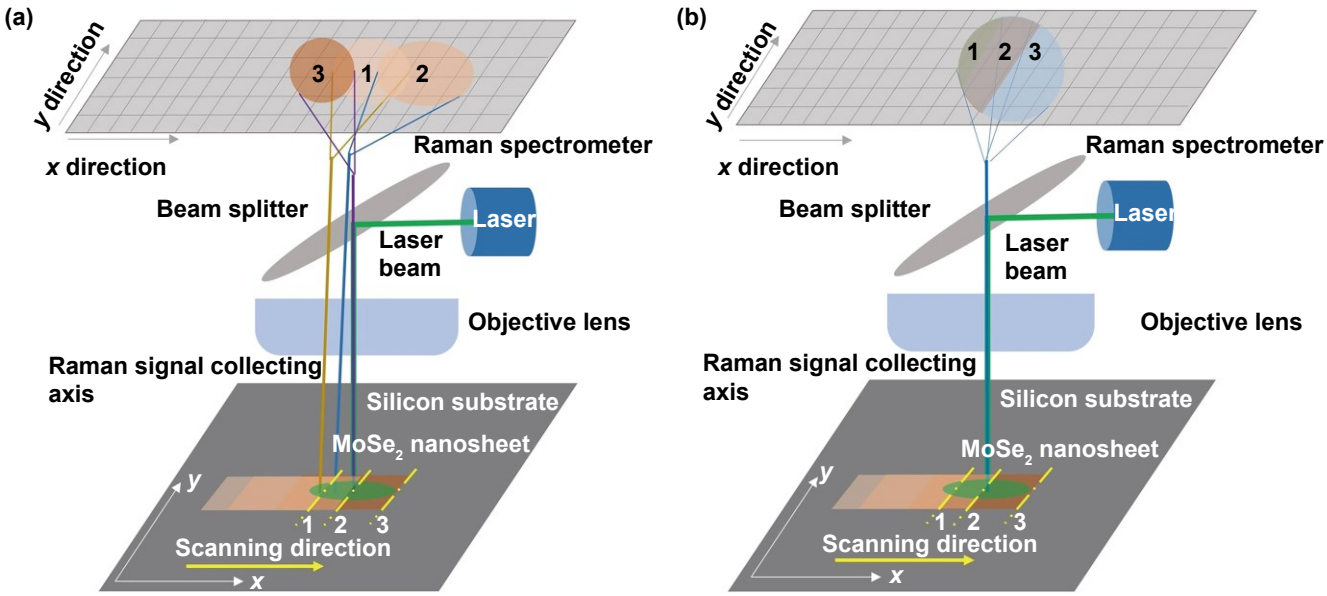


Figure 9. Schematic of the scanning Raman system used to detect the Raman signal of (a) silicon substrate and (b) $MoSe_2$ nanosheet.[82]

## 4. Raman-based Thermal Probing: Transient Response

As mentioned previously, for thermocouple, the time response of this technique is not fast enough to realize the real-time temperature detection of materials under laser heating. And infrared thermometry technique is hard to measure the transient response of the sample under ultrafast laser pulse heating or for nanoscale regions.

As an optical technique, the pump-probe thermoreflectance technique can be used to measure heat transfer in bulk materials and micro/nanoscale samples. In this technique, two lasers are used as the pump and probe, respectively. The pump beam irradiates the sample to generate a time-dependent heat flux, while the probe beam is used to characterize the temperature response through a proportional change in surface reflectivity. Then, the thermal properties, which include the cross-plane and in-plane thermal conductivities, heat capacity, and thermal boundary conductance between materials, can be determined by combining with a heat transfer model.[83] Though pump-probe thermoreflectance is able to probe the material's thermal response, a thin layer of metal is usually needed to coat the samples, especially for some samples with rough surface. This metal layer, which is opaque at both pump and probe wavelengths and has a large coefficient of thermoreflectance at the probe wavelength, is taken as transducer layer. In addition, the technique is a relative measurement method, which indicates that the accuracy will be lower. And this technique also cannot be used in situations with extremely high temperature.

Raman spectroscopy can also be used for fast or ultrafast thermal response probing, which is very critical for understanding the transient thermal response of materials in laser extreme manufacturing. One way is to use a single pulsed laser for both laser heating and Raman signal excitation. Wang's group has developed a technique named energy transport state resolved Raman (ET-Raman) for probing thermal transport in 2D materials. In this technique, different energy transport states in both space and time domains are constructed to probe a materials' thermal response for different situations.[62, 84-86] As shown in Fig. 10, under laser heating, three physical processes take place, which all affect the thermal response of the sample. The first one is hot carrier

generation, diffusion in space, and electron-hole recombination. This process, which introduces heat transfer and energy redistribution, is determined by the hot carrier diffusivity. Subsequently, phonons, which receive energy from hot carriers or electron-hole recombination, conduct the heat in the 2D materials. This heat conduction is mainly related to the in-plane thermal conductivity of 2D materials. Finally, the heat is conducted from 2D materials to the substrate, and this process is dominated by the local thermal resistance. By using a novel five-state ET-Raman method, the critical effects of hot carrier diffusion, electron-hole recombination, and energy coupling with phonons are taken into consideration when determining the thermal conductivity of supported 2D materials for the first time.[62] Although this work is focused on supported 2D materials, the thermal transport of suspended 2D materials can also be explored by using the ET-Raman method. For supported samples, the thermal conductivity of some substrates, such as silicon, is very high, which indicates that the thermal transport will reach steady state very soon. As a result, a picosecond laser is used to construct the transient energy transport state. However, this picosecond laser cannot be used for suspended samples since the pulse interval is so short that a strong heat accumulation effect will happen and could destroy the sample. A nanosecond laser can be used instead.[85-86] Although the ET-Raman technique is focused on thermal transport study, it provides a novel way to probing a material's thermal response under ultrafast laser heating.

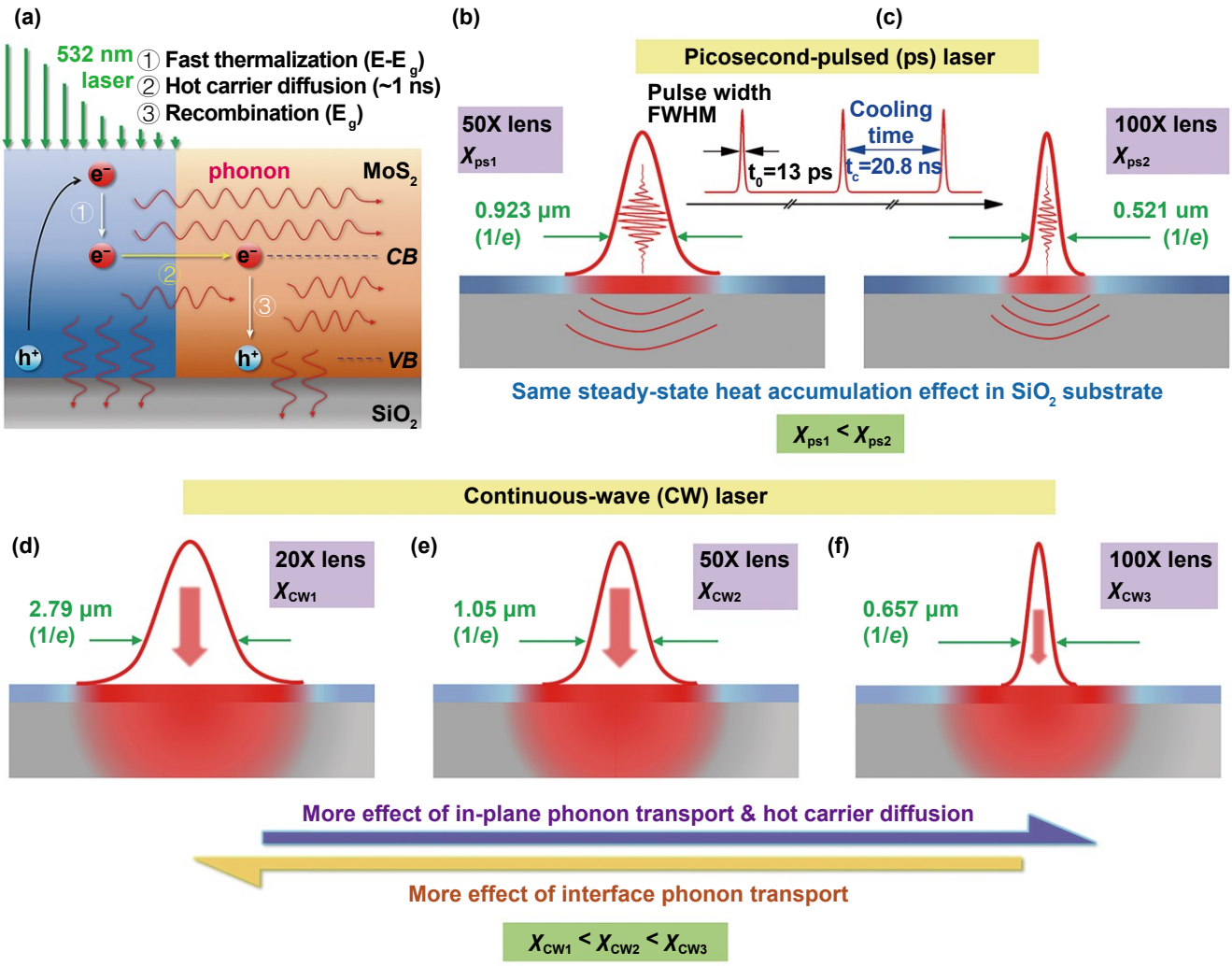


Figure 10. The schematic for the physical principle of five-state picosecond ET-Raman technique. (a) The generation, diffusion of hot carrier, and electron-hole recombination. (b, c) Two sub-states in ps laser heating under 50× and 100× objective lenses. (d-f) Three sub-states in CW laser heating under 20×, 50×, and 100× objective lenses.[62]

Raman pump-probe spectroscopy can be an alternative technique. Similarly, in this technique, two pulsed lasers are used: one laser for designated laser heating and manufacturing, and another laser for Raman excitation. The time delay of the two lasers can be adjusted using the same manner in the pump-probe technique. In this technique, a strong pump pulse is focused onto the sample to create a time-dependent heat flux, while a weak time-delayed probe pulse monitors the response of the surface temperature through Raman transitions.[87]

For many laser extreme manufacturing situations, the temperature could be very high, which makes the Raman signal extremely low. To enhance the signal significantly, two special Raman techniques, stimulated Raman scattering (SRS) and coherent anti-Stokes Raman scattering (CARS), can be employed. SRS is a coherent Raman scattering technique, and the signals are generated by the co-alignment of two incident beams (the pump and Stokes beams), as shown in Fig. 11. By tuning the frequency difference between the two beams to match a molecular vibration, stimulated excitation of the Raman active molecular vibration occurs. As a result of the coherent excitation of a molecular vibration, a pump photon is absorbed by the sample and a Stokes photon is generated. This results in stimulated Raman loss (SRL) and stimulated Raman gain (SRG), respectively. And these two signals are proportional to the number of molecules in the probe volume and the molecular Raman scattering cross-section. As all the vibrational modes are prepared in a coherent fashion, these modes oscillate in unison to form a coherent polarization in the sample, and the subsequent radiation derived from the polarization is also coherent. The resulting SRS radiation is highly directional and strong, boosting vibrational excitation by a factor of $10^7$, offering signal detection efficiencies that are many orders of magnitude higher than spontaneous Raman scattering. In addition, SRS technique enables direct observation of the coherent molecular motions at ultrafast time scale, following their evolution and dephasing as a function of time. This allows for a time-resolved view of processes and molecular dynamics that cannot always by directly inferred from an analysis of the Raman spectra alone. SRS is also used to measure the temperature of condensed matter at the molecular vibrational level.[88]

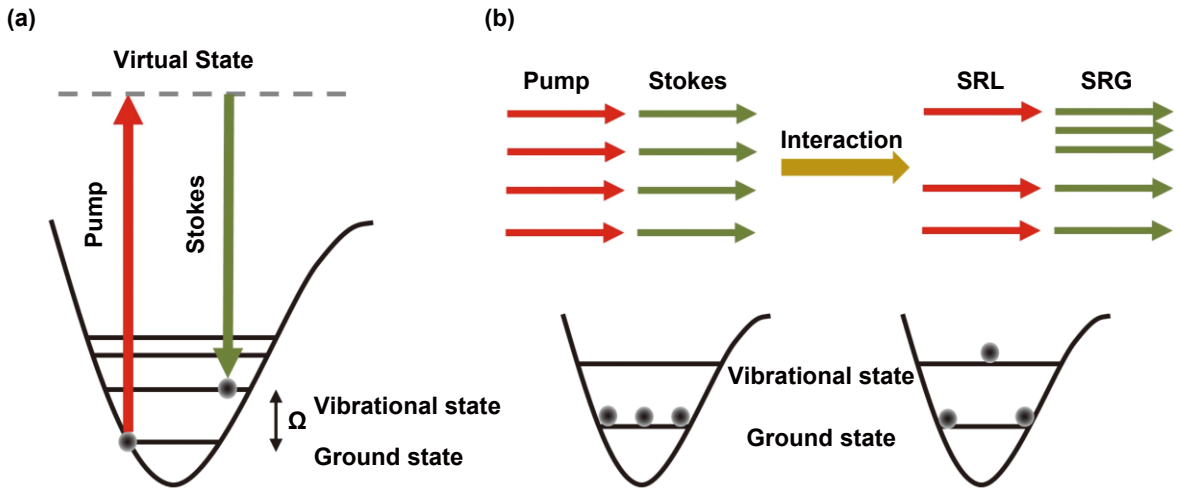


Figure 11. Principle of stimulated Raman scattering. (a) Energy diagram of SRS. (b) Output spectrum associated with SRS process.

The other method to significantly enhance the Raman signal is CARS. This method is a nonlinear variant of Raman spectroscopy which combines signal enhancement by more than four orders of magnitude with further advantages such as directional emission, and narrow spectral bandwidth.[89-91] CARS is consisted of two stimulated Raman scattering steps. First, a pump photon with a frequency of $\omega_p$ and a Stokes photon with a frequency of $\omega_s$ resonantly excite a Raman oscillator with a vibrational frequency of $\Omega = \omega_p - \omega_s$. Then, the Raman oscillator is de-excited by a probe photon with a frequency of $\omega_{pr}$ to produce an anti-Stokes photon with a frequency of $\omega_{as} = \omega_{pr} + \Omega$. The energy diagram and molecular illustration of the CARS process are shown in Fig. 12.[92] An important advantage of CARS over spontaneous Raman scattering is that background fluorescence from the samples does not interfere with the CARS signal detection. And, because of the coherent property, the CARS signal increases quadratically with respect to the number of vibrational oscillators in the focal volume. This technique has been used widely to obtain gas-phase temperature because of its high accuracy, precision, relative insensitivity to the collisional environment, and because it can be applied even in high luminous flames.[93]

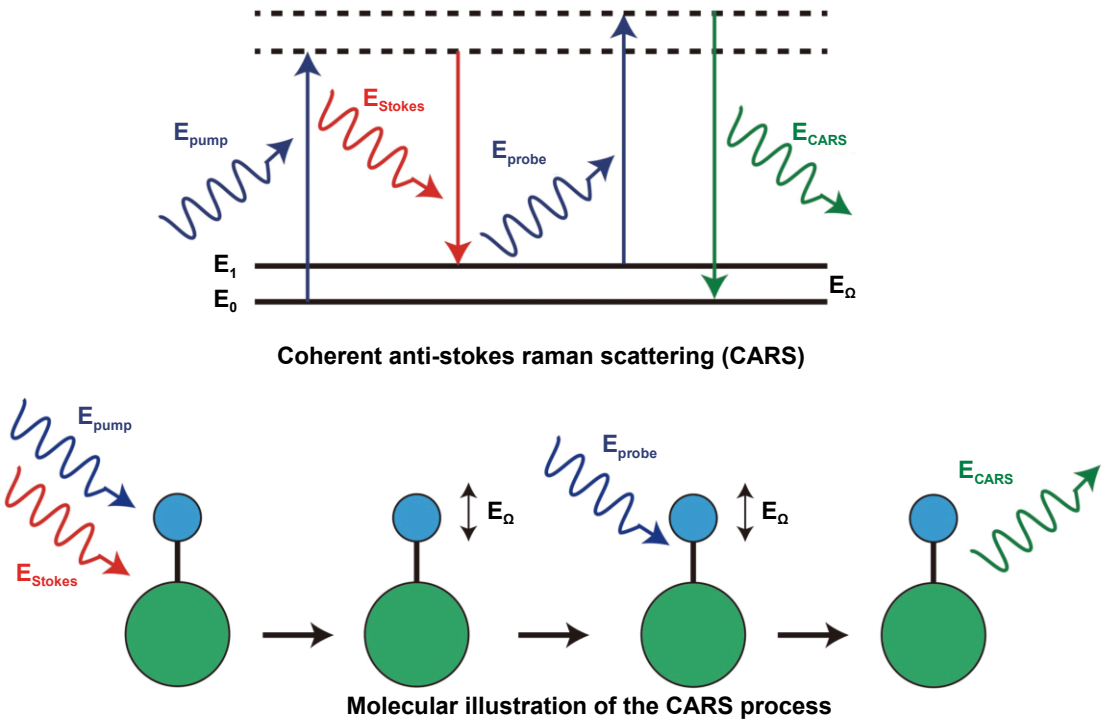


Figure 12. Energy diagram and molecular illustration of the CARS process[92]

## 5. Concluding Remarks and Outlook

As all the LAM processes involve intensive heating, it is very crucial to probe the materials' thermal response to understand the physics behind these processes, including laser absorption, heating, heat conduction, melting, vaporization, and crystallization/solidification. Raman spectroscopy can be taken as a novel way to measuring temperature during laser-assisted extreme manufacturing. In this review, the basic mechanisms of Raman-based temperature probing were introduced. Various Raman-based techniques used for temperature probing, including near-field Raman thermometry, ET-Raman, pump-probe Raman technique, SRS method and CARS method were critically reviewed for their measurement mechanism as well as their applications.

In laser-assisted extreme manufacturing, extreme stress usually accompanies the very high elevated temperature. As a result, great caution must be taken when using Raman wavenumber for

temperature measurement as it can also be strongly affected by the local stress. Combined use of Raman wavenumber and linewidth is highly recommended to distinguish and measure temperature and stress. In spontaneous Raman spectroscopy, the focal level and surface morphology/structure (even at the scale of tens of nm) could strongly alter the optical path of the Raman signal back to the detector, and induce undesired Raman properties change. This type of surface-induced change sometimes is embedded in the temperature-induced Raman properties change, and should be carefully considered in order to obtain physically reasonable information on local temperature rise.

In some LAM processes, for instance laser peening and laser nanoimprinting, there are not many pathways to characterize temperature of the target during the manufacturing process because of the nanoscale geometry as well as the high heating density. Raman thermometry can be used in such scenario, not just because of its non-contact nature but also because of its enhanced signal due to the near-field effect. And in many LAM processes, such as laser-assisted cutting, laser peening, etc., the temperature could be very high, and it makes the Raman signal extremely low. SRS and CARS could enhance the Raman signal dramatically to realize temperature probing in such manufacturing processes. As Raman spectra can also be used to characterize the structure variation of the sample, these Raman-based techniques are very good candidates for characterization of structure variation of materials during manufacturing processes.

In laser-assisted extreme manufacturing, if the target material is not Raman active (e.g. metals), a Raman active material can be placed in the manufacturing region for temperature probing. For instance, some high temperature-resistant materials, like diamond nanoparticles and graphene can be used for very efficient Raman signal excitation and ultrafast probing due to the sensor's

extremely small thermal inertia. It needs to be pointed out that even without near-field focusing, the temperature probing resolution can still be well beyond the diffraction limit by using nanoscale Raman sensing materials/structures whose feature size is significantly smaller than the focal spot.

Additionally, in many LAM processes, the temperature variation of material is very fast (even in picoseconds). In such situations, Raman techniques with a picosecond/femtosecond pulsed laser can be used to explore the transient thermal response of materials and the possible structure variation during such short heating process. As the laser spot size is controllable, this technique can also realize a high spatial resolution at the same time. As a result, the Raman technique is a very promising one for probing the thermal response of materials with very high resolution in time and space domains.

**Acknowledgement**

We are grateful to the financial support of National Key R&D Program of China (No. 2018YFE0205000 and No.2019YFA0905800 for R.W.), Program for Professor of Special Appointment (Eastern Scholar) at Shanghai Institutions of Higher Learning and China Scholarship Council (S.X.), National Natural Science Foundation of China (No. 5157614 for Y.Y.) and U.S. National Science Foundation (CBET1930866 for X.W.).

## References


1. Kim, K.-S.; Kim, J.-H.; Choi, J.-Y.; Lee, C.-M., A review on research and development of laser assisted turning. *International Journal of Precision Engineering and Manufacturing* **2011,** *12* (4), 753-759.
2. Dutta Majumdar, J.; Manna, I., Laser material processing. *International Materials Reviews* **2011,** *56* (5-6), 341-388.
3. Zhao, L.; Cheng, J.; Chen, M.; Yuan, X.; Liao, W.; Liu, Q.; Yang, H.; Wang, H., Formation mechanism of a smooth, defect-free surface of fused silica optics using rapid CO2 laser polishing. *International Journal of Extreme Manufacturing* **2019,** *1* (3), 035001.
4. Cvecek, K.; Dehmel, S.; Miyamoto, I.; Schmidt, M., A review on glass welding by ultra-short laser pulses. *International Journal of Extreme Manufacturing* **2019,** *1* (4), 042001.
5. Gautam, G. D.; Pandey, A. K., Pulsed Nd:YAG laser beam drilling: A review. *Optics & Laser Technology* **2018,** *100*, 183-215.
6. Dewil, R.; Vansteenwegen, P.; Cattrysse, D., A review of cutting path algorithms for laser cutters. *The International Journal of Advanced Manufacturing Technology* **2016,** *87* (5), 1865-1884.
7. Yocom, C. J.; Zhang, X.; Liao, Y., Research and development status of laser peen forming: A review. *Optics & Laser Technology* **2018,** *108*, 32-45.
8. Barner-Kowollik, C.; Bastmeyer, M.; Blasco, E.; Delaittre, G.; Müller, P.; Richter, B.; Wegener, M., 3D Laser Micro- and Nanoprinting: Challenges for Chemistry. *Angewandte Chemie International Edition* **2017,** *56* (50), 15828-15845.
9. Gu, D. D.; Meiners, W.; Wissenbach, K.; Poprawe, R., Laser additive manufacturing of metallic components: materials, processes and mechanisms. *International Materials Reviews* **2012,** *57* (3), 133-164.
10. Chimmalgi, A.; Grigoropoulos, C. P.; Komvopoulos, K., Surface nanostructuring by nano-/femtosecond laser-assisted scanning force microscopy. *J Appl Phys* **2005,** *97* (10), 104319.
11. Meijer, J., Laser beam machining (LBM), state of the art and new opportunities. *Journal of Materials Processing Technology* **2004,** *149* (1), 2-17.
12. Dubey, A. K.; Yadava, V., Laser beam machining—A review. *International Journal of Machine Tools and Manufacture* **2008,** *48* (6), 609-628.
13. Arrizubieta, J. I.; Klocke, F.; Gräfe, S.; Arntz, K.; Lamikiz, A., Thermal Simulation of Laser-assisted Turning. *Procedia Engineering* **2015,** *132*, 639-646.
14. Dhakal, B.; Swaroop, S., Review: Laser shock peening as post welding treatment technique. *Journal of Manufacturing Processes* **2018,** *32*, 721-733.
15. Gujba, K. A.; Medraj, M., Laser Peening Process and Its Impact on Materials Properties in Comparison with Shot Peening and Ultrasonic Impact Peening. *Materials (Basel)* **2014,** *7* (12), 7925-7974.
16. Montross, C. S.; Wei, T.; Ye, L.; Clark, G.; Mai, Y.-W., Laser shock processing and its effects on microstructure and properties of metal alloys: a review. *International Journal of Fatigue* **2002,** *24* (10), 1021-1036.
17. Zhang, X. C.; Zhang, Y. K.; Lu, J. Z.; Xuan, F. Z.; Wang, Z. D.; Tu, S. T., Improvement of fatigue life of Ti–6Al–4V alloy by laser shock peening. *Materials Science and Engineering: A* **2010,** *527* (15), 3411-3415.
18. Hsiao, F. B.; Jen, C. P.; Wang, D. B.; Chuang, C. H.; Lee, Y. C.; Liu, C. P.; Hsu, H. J., An analytical modeling of heat transfer for laser-assisted nanoimprinting processes. *Computational Mechanics* **2006,** *37* (2), 173-181.
19. Ahmadi, Z.; Yakupoglu, B.; Azam, N.; Elafandi, S.; Mahjouri-Samani, M., Self-limiting laser crystallization and direct writing of 2D materials. *International Journal of Extreme Manufacturing* **2019,** *1* (1), 015001.

20. Li, L. P.; Lu, Y. F.; Doerr, D. W.; Alexander, D. R.; Shi, J.; Li, J. C., Fabrication of hemispherical cavity arrays on silicon substrates using laser-assisted nanoimprinting of self-assembled particles. *Nanotechnology* **2003,** *15* (3), 333-336.
21. Wu, G.; Hu, Y.; Zhu, W.; Song, C.; Han, H. In *Research Status and Development Trend of Laser Additive Manufacturing Technology*, 2017 4th International Conference on Information Science and Control Engineering (ICISCE), Changsha, China, 21-23 July 2017; IEEE: Changsha, China, 2017; pp 1210-1213.
22. Melchels, F. P. W.; Domingos, M. A. N.; Klein, T. J.; Malda, J.; Bartolo, P. J.; Hutmacher, D. W., Additive manufacturing of tissues and organs. *Progress in Polymer Science* **2012,** *37* (8), 1079-1104.
23. Buchbinder, D.; Schleifenbaum, H.; Heidrich, S.; Meiners, W.; Bültmann, J., High Power Selective Laser Melting (HP SLM) of Aluminum Parts. *Physics Procedia* **2011,** *12*, 271-278.
24. Baufeld, B.; Biest, O. V. d.; Gault, R., Additive manufacturing of Ti–6Al–4V components by shaped metal deposition: Microstructure and mechanical properties. *Materials & Design* **2010,** *31*, S106-S111.
25. Murr, L. E.; Martinez, E.; Amato, K. N.; Gaytan, S. M.; Hernandez, J.; Ramirez, D. A.; Shindo, P. W.; Medina, F.; Wicker, R. B., Fabrication of Metal and Alloy Components by Additive Manufacturing: Examples of 3D Materials Science. *Journal of Materials Research and Technology* **2012,** *1* (1), 42-54.
26. Wang, X., Large-scale molecular dynamics simulation of surface nanostructuring with a laser-assisted scanning tunnelling microscope. *Journal of Physics D: Applied Physics* **2005,** *38* (11), 1805-1823.
27. Jersch, J.; Demming, F.; Dickmann, K., Nanostructuring with laser radiation in the nearfield of a tip from a scanning force microscope. *Applied Physics A* **1996,** *64* (1), 29-32.
28. Xu, S.; Zhang, L.; Yue, Y.; Wang, X., Physics in Laser Near-Field Nanomanufacturing: Fundamental Understanding and Novel Probing. In *Encyclopedia of Nanotechnology*, Bhushan, B., Ed. Springer Netherlands: Dordrecht, 2016; pp 3195-3213.
29. Mai, Z. H.; Lu, Y. F.; Huang, S. M.; Chim, W. K.; Pan, J. S., Mechanism of laser-induced nanomodification on hydrogen-passivated Si(100) surfaces underneath the tip of a scanning tunneling microscope. *Journal of Vacuum Science & Technology B: Microelectronics and Nanometer Structures Processing, Measurement, and Phenomena* **2000,** *18* (4), 1853-1857.
30. Mai, Z. H.; Lu, Y. F.; Song, W. D.; Chim, W. K., Nano-modification on hydrogen-passivated Si surfaces by a laser-assisted scanning tunneling microscope operating in air. *Appl Surf Sci* **2000,** *154-155*, 360-364.
31. Kim, M. M.; Giry, A.; Mastiani, M.; Rodrigues, G. O.; Reis, A.; Mandin, P., Microscale thermometry: A review. *Microelectronic Engineering* **2015,** *148*, 129-142.
32. Hetsroni, G.; Mosyak, A.; Pogrebnyak, E.; Rozenblit, R., Infrared temperature measurements in micro-channels and micro-fluid systems. *International Journal of Thermal Sciences* **2011,** *50* (6), 853-868.
33. Astarita, T.; Cardone, G.; Carlomagno, G. M.; Meola, C., A survey on infrared thermography for convective heat transfer measurements. *Optics & Laser Technology* **2000,** *32* (7), 593-610.
34. Tian, B.; Zhang, Z.; Shi, P.; Zheng, C.; Yu, Q.; Jing, W.; Jiang, Z., Tungsten-rhenium thin film thermocouples for SiC-based ceramic matrix composites. *Rev Sci Instrum* **2017,** *88* (1), 015007.
35. Kölbl, N.; Marschall, I.; Harmuth, H., High-temperature investigation of mould slag crystallization by single and double hot thermocouple techniques. *Journal of Iron and Steel Research International* **2019,** *26* (4), 345-354.
36. Tougas, M. I.; Amani, M.; Gregory, J. O., Metallic and Ceramic Thin Film Thermocouples for Gas Turbine Engines. *Sensors* **2013,** *13* (11), 15324-15347.
37. Sonibare, O. O.; Haeger, T.; Foley, S. F., Structural characterization of Nigerian coals by X-ray diffraction, Raman and FTIR spectroscopy. *Energy* **2010,** *35* (12), 5347-5353.
38. He, X.; Liu, X.; Nie, B.; Song, D., FTIR and Raman spectroscopy characterization of functional groups in various rank coals. *Fuel* **2017,** *206*, 555-563.

39. Yue, Y.; Wang, X., Nanoscale thermal probing. *Nano Rev* **2012,** *3* (1), 11586.
40. Xu, S.; Wang, T.; Hurley, D.; Yue, Y.; Wang, X., Development of time-domain differential Raman for transient thermal probing of materials. *Opt. Express* **2015,** *23* (8), 10040-10056.
41. Serrano, J. R.; Phinney, L. M.; Kearney, S. P., Micro-Raman thermometry of thermal flexure actuators. *Journal of Micromechanics and Microengineering* **2006,** *16* (7), 1128-1134.
42. Kittel, C., *Introduction to Solid State Physics*. Wiley: New York, 2004.
43. Attal-Trétout, B.; Bouchardy, P.; Magre, P.; Péalat, M.; Taran, J. P., CARS in combustion: Prospects and problems. *Applied Physics B* **1990,** *51* (1), 17-24.
44. Harris, D. C.; Bertolucci, M. D., *Symmetry and Spectroscopy: An Introduction to Vibrational and Electronic Spectroscopy*. 1st ed.; Oxford University Press: New York, 1978.
45. Cialla-May, D.; Schmitt, M.; Popp, J., Theoretical principles of Raman spectroscopy. *Physical Sciences Reviews* **2019,** *4* (6), 20170040.
46. Das, R. S.; Agrawal, Y. K., Raman spectroscopy: Recent advancements, techniques and applications. *Vib Spectrosc* **2011,** *57* (2), 163-176.
47. Childs, P. R. N.; Greenwood, J. R.; Long, C. A., Review of temperature measurement. *Rev Sci Instrum* **2000,** *71* (8), 2959-2978.
48. Xu, Z.; He, Z.; Song, Y.; Fu, X.; Rommel, M.; Luo, X.; Hartmaier, A.; Zhang, J.; Fang, F., Topic Review: Application of Raman Spectroscopy Characterization in Micro/Nano-Machining. *Micromachines* **2018,** *9* (7), 361.
49. Yue, Y. N.; Zhang, J. C.; Wang, X. W., Micro/Nanoscale Spatial Resolution Temperature Probing for the Interfacial Thermal Characterization of Epitaxial Graphene on 4H-SiC. *Small* **2011,** *7* (23), 3324-3333.
50. Wallis, R. F.; Balkanski, M., *Many-body Aspects of Solid State Spectroscopy*. North-Holland Physics: Amsterdam, 1986.
51. Weber, W. H.; Merlin, R., *Raman Scattering in Materials Science*. Springer: New York, 2000.
52. Hosoya, N.; Akaho, Y.; Inoue, M.; Sahoo, S.; Tachibana, M., Temperature dependence of the Raman spectra of polycrystalline graphene grown by chemical vapor deposition. *Appl Phys Lett* **2014,** *105* (2), 023108.
53. Huang, X.; Gao, Y.; Yang, T.; Ren, W.; Cheng, H.-M.; Lai, T., Quantitative Analysis of Temperature Dependence of Raman shift of monolayer $WS_2$. *Sci Rep* **2016,** *6* (1), 32236.
54. Hart, T. R.; Aggarwal, R. L.; Lax, B., Temperature Dependence of Raman Scattering in Silicon. *Physical Review B* **1970,** *1* (2), 638-642.
55. John, N.; George, S., Chapter 5 - Raman Spectroscopy. In *Spectroscopic Methods for Nanomaterials Characterization*, Thomas, S.; Thomas, R.; Zachariah, A. K.; Mishra, R. K., Eds. Elsevier: 2017; pp 95-127.
56. Sun, H. Y.; Xu, Z.; Gao, C., Multifunctional, Ultra-Flyweight, Synergistically Assembled Carbon Aerogels. *Advanced Materials* **2013,** *25* (18), 2554-2560.
57. Tang, X.; Xu, S.; Wang, X., Thermal probing in single microparticle and microfiber induced near-field laser focusing. *Opt. Express* **2013,** *21* (12), 14303-14315.
58. Wang, Z. L.; Tang, D. W., Investigation of heat transfer around microwire in air environment using 3ω method. *International Journal of Thermal Sciences* **2013,** *64*, 145-151.
59. Rumble, J. R., *CRC Handbook of Chemistry and Physics*. 100th ed.; CRC Press: 2019.
60. Yuan, P.; Li, C.; Xu, S.; Liu, J.; Wang, X., Interfacial thermal conductance between few to tens of layered-MoS 2 and c-Si: Effect of MoS 2 thickness. *Acta Materialia* **2017,** *122*, 152-165.
61. Yuan, P.; Liu, J.; Wang, R.; Wang, X., The hot carrier diffusion coefficient of sub-10 nm virgin $MoS_2$: uncovered by non-contact optical probing. *Nanoscale* **2017,** *9* (20), 6808-6020.

62. Yuan, P.; Wang, R.; Wang, T.; Wang, X.; Xie, Y., Nonmonotonic thickness-dependence of in-plane thermal conductivity of few-layered MoS2: 2.4 to 37.8 nm. *Physical Chemistry Chemical Physics* **2018,** *20* (40), 25752-25761.
63. Tang, X.; Xu, S.; Wang, X., Corrugated epitaxial graphene/SiC interfaces: photon excitation and probing. *Nanoscale* **2014,** *6* (15), 8822-8830.
64. van de Burgt, Y., Laser-assisted growth of carbon nanotubes—A review. *Journal of Laser Applications* **2014,** *26* (3), 032001.
65. Tofail, S. A. M.; Koumoulos, E. P.; Bandyopadhyay, A.; Bose, S.; O'Donoghue, L.; Charitidis, C., Additive manufacturing: scientific and technological challenges, market uptake and opportunities. *Materials Today* **2018,** *21* (1), 22-37.
66. Tang, X.; Xu, S.; Zhang, J.; Wang, X., Five Orders of Magnitude Reduction in Energy Coupling across Corrugated Graphene/Substrate Interfaces. *ACS Applied Materials & Interfaces* **2014,** *6* (4), 2809-2818.
67. Zhou, H.; Qiu, C.; Yu, F.; Yang, H.; Chen, M.; Hu, L.; Guo, Y.; Sun, L., Raman scattering of monolayer graphene: the temperature and oxygen doping effects. *Journal of Physics D: Applied Physics* **2011,** *44* (18), 185404.
68. Zhang, L.; Jia, Z.; Huang, L.; O'Brien, S.; Yu, Z., Low-Temperature Raman Spectroscopy of Individual Single-Wall Carbon Nanotubes and Single-Layer Graphene. *The Journal of Physical Chemistry C* **2008,** *112* (36), 13893-13900.
69. Allen, M. J.; Fowler, J. D.; Tung, V. C.; Yang, Y.; Weiller, B. H.; Kaner, R. B., Temperature dependent Raman spectroscopy of chemically derived graphene. *Appl Phys Lett* **2008,** *93* (19), 193119.
70. Calizo, I.; Balandin, A. A.; Bao, W.; Miao, F.; Lau, C. N., Temperature Dependence of the Raman Spectra of Graphene and Graphene Multilayers. *Nano Lett* **2007,** *7* (9), 2645-2649.
71. Balandin, A. A., Thermal properties of graphene and nanostructured carbon materials. *Nature Materials* **2011,** *10* (8), 569-581.
72. Zhao, W.; Chen, W.; Yue, Y.; Wu, S., In-situ two-step Raman thermometry for thermal characterization of monolayer graphene interface material. *Applied Thermal Engineering* **2017,** *113*, 481-489.
73. Wang, W.; Peng, Q.; Dai, Y.; Qian, Z.; Liu, S., Temperature dependence of Raman spectra of graphene on copper foil substrate. *Journal of Materials Science: Materials in Electronics* **2016,** *27* (4), 3888-3893.
74. Malard, L. M.; Nilsson, J.; Mafra, D. L.; Elias, D. C.; Brant, J. C.; Plentz, F.; Alves, E. S.; Neto, A. H. C.; Pimenta, M. A., Electronic properties of bilayer graphene probed by Resonance Raman Scattering. *physica status solidi (b)* **2008,** *245* (10), 2060-2063.
75. Yue, Y.; Chen, X.; Wang, X., Noncontact Sub-10 nm Temperature Measurement in Near-Field Laser Heating. *ACS nano* **2011,** *5* (6), 4466-4475.
76. Chen, X.; Wang, X., Near-field thermal transport in a nanotip under laser irradiation. *Nanotechnology* **2011,** *22* (7), 075204.
77. Chen, X.; Wang, X., Microscale spatially resolved thermal response of Si nanotip to laser irradiation. *The Journal of Physical Chemistry C* **2011,** *115* (45), 22207-22216.
78. Kucsko, G.; Maurer, P. C.; Yao, N. Y.; Kubo, M.; Noh, H. J.; Lo, P. K.; Park, H.; Lukin, M. D., Nanometre-scale thermometry in a living cell. *Nature* **2013,** *500* (7460), 54-58.
79. Li, C.; Yue, Y., Fluorescence spectroscopy of graphene quantum dots: temperature effect at different excitation wavelengths. *Nanotechnology* **2014,** *25* (43), 435703.
80. Neumann, P.; Jakobi, I.; Dolde, F.; Burk, C.; Reuter, R.; Waldherr, G.; Honert, J.; Wolf, T.; Brunner, A.; Shim, J. H.; Suter, D.; Sumiya, H.; Isoya, J.; Wrachtrup, J., High-Precision Nanoscale Temperature Sensing Using Single Defects in Diamond. *Nano Lett* **2013,** *13* (6), 2738-2742.

81. Tang, X.; Xu, S.; Wang, X., Nanoscale Probing of Thermal, Stress, and Optical Fields under Near-Field Laser Heating. *PLoS ONE* **2013,** *8* (3), e58030.
82. Wang, R.; Yuan, P.; Han, M.; Xu, S.; Wang, T.; Wang, X., Asymmetry of Raman scattering by structure variation in space. *Opt. Express* **2017,** *25* (15), 18378-18392.
83. Schmidt, A. J., pump probe thermoreflectance. *Annual Review of Heat Transfer* **2013,** *16*, 159-181.
84. Yuan, P.; Wang, R.; Tan, H.; Wang, T.; Wang, X., Energy Transport State Resolved Raman for Probing Interface Energy Transport and Hot Carrier Diffusion in Few-Layered $MoS_2$. *ACS Photonics* **2017,** *4* (12), 3115-3129.
85. Wang, R.; Wang, T.; Zobeiri, H.; Yuan, P.; Deng, C.; Yue, Y.; Xu, S.; Wang, X., Measurement of the thermal conductivities of suspended $MoS_2$ and $MoSe_2$ by nanosecond ET-Raman without temperature calibration and laser absorption evaluation. *Nanoscale* **2018,** *10* (48), 23087-23102.
86. Zobeiri, H.; Wang, R.; Zhang, Q.; Zhu, G.; Wang, X., Hot carrier transfer and phonon transport in suspended nm $WS_2$ films. *Acta Materialia* **2019,** *175*, 222-237.
87. Souther, N.; Wagner, R.; Harnish, P.; Briel, M.; Bali, S., Measurements of light shifts in cold atoms using Raman pump-probe spectroscopy. *Laser Physics Letters* **2010,** *7* (4), 321-327.
88. Dang, N. C.; Bolme, C. A.; Moore, D. S.; McGrane, S. D., Femtosecond Stimulated Raman Scattering Picosecond Molecular Thermometry in Condensed Phases. *Phys Rev Lett* **2011,** *107* (4), 043001.
89. Müller, M.; Zumbusch, A., Coherent anti-Stokes Raman Scattering Microscopy. *ChemPhysChem* **2007,** *8* (15), 2156-2170.
90. Krafft, C.; Dietzek, B.; Popp, J., Raman and CARSmicrospectroscopy of cells and tissues. *Analyst* **2009,** *134* (6), 1046-1057.
91. Tu, H.; Boppart, S. A., Coherent anti-Stokes Raman scattering microscopy: overcoming technical barriers for clinical translation. *Journal of Biophotonics* **2014,** *7* (1‐2), 9-22.
92. Lei, T. C.; Ammar, D. A.; Masihzadeh, O.; Gibson, E. A.; Kahook, M. Y., Label-free imaging of trabecular meshwork cells using Coherent Anti-Stokes Raman Scattering (CARS) microscopy. *Molecular vision* **2011,** *17*, 2628-2633.
93. Dennis, C. N.; Satija, A.; Lucht, R. P., High dynamic range thermometry at 5 kHz in hydrogen–air diffusion flame using chirped-probe-pulse femtosecond coherent anti-stokes Raman scattering. *Journal of Raman Spectroscopy* **2016,** *47* (2), 177-188.